Dyes and Pigments 220 (2023) 111722

Contents lists available at ScienceDirect

Dyes and Pigments

journal homepage: www.elsevier.com/locate/dyepig

Luminescent blue emissive bis(alkynyl) borane compounds with a *N*, *O*-coordinated ligand

Gioele Colombo [a], Anita Cinco [a,b], Stefano Brenna [a,*], Julien Furrer [c], Bruno Therrien [d], G. Attilio Ardizzoia [a]

[a] *Dipartimento di Scienza e Alta Tecnologia, Università degli Studi dell'Insubria and CIRCC, Via Valleggio, 9, 22100, Como, Italy*
[b] *University School for Advanced Studies IUSS Pavia, Italy*
[c] *Departement für Chemie, Biochemie und Pharmazie, Universität Bern, Freiestrasse 3, CH-3012, Bern, Switzerland*
[d] *Institute of Chemistry, Université de Neuchâtel, Avenue de Bellevaux 51, CH-2000, Neuchâtel, Switzerland*

ARTICLE INFO

Keywords:
Imidazo[1,5-*a*]pyridines
Fluorescence
Alkynyl compounds
Blue emission
Boron

ABSTRACT

Five bis(alkynyl)boranes with a (imidazo[1,5-*a*]pyridin-3-yl)phenolate ligand have been synthesized and characterized both in solution (^{1}H, ^{13}C, ^{11}B, ^{19}F NMR) and in the solid state (X-ray). All derivatives, differing for the substituent R (H, Me, OMe, CF_3, NMe_2) in the para position of the phenylacetylene moieties, displayed blue fluorescence emission in solution, linearly correlated to the electronic properties of the substituent R (i.e., its σ_p Hammett constant). High Stokes shifts and good quantum yields were recorded. Time-Dependent Density Functional Theory (TD-DFT) calculations were performed to describe the percentage contribution of each fragment of the molecule to the frontier orbitals. Electron Density Difference Maps (EDDMs) calculated for all derivatives allowed to explain the emissive properties of the studied compounds.

1. Introduction

Luminescent boron compounds have received great attention in the last decades due to their potential applications as stimuli-responsive materials [1], emissive layer in Organic Light Emitting Diodes (OLEDs) [2–5], anion sensors [6] or bioimaging probes [7,8]. Such performances are observed either in tricoordinate [6,7] or tetracoordinate boron species [2]. Among the latter, significant consideration has been devoted to BF_2-containing compounds, in particular to the ubiquitous 4,4-difluoro-4-bora-3a,4a-diaza-*s*-indacene, more known as boron dipyrromethene (BODIPY) [9], which gained a lot of interest owing to very high quantum yields, excellent chemical stability in solution and in solid state and the possibility to finely tune the electronic properties. Sometimes, a limitation of BODIPY dyes lies in a certain instability under irradiation or sensitivity to polar solvents due to the presence of B-F bonds [2]. One possible strategy to overcome this problem is the substitution of the fluorine atoms with aryl or alkynyl groups, the resulting organo-boron compounds showing higher stability and better photophysical performances. Among others, bis(alkynyl) borane compounds proved to be very successful in this regard. In the literature, there are several reports on (*N*,*N*)B(alkynyl)$_2$ compounds [10–18], with BODIPY being the most employed bidentate *N*,*N*-ligand: to cite the most recent examples, Hupp [17] synthesized porous organic polymers with photocatalytic activity in oxidation reactions starting from the BODIPY-based monomer *N*,*N*-**I** (Fig. 1); whereas Ema [16] prepared the wide class of carbazole-based BODIPYs *N*,*N*-**II** which showed interesting solid state fluorescence. Finally, Ortiz [15] demonstrated how the substitution of fluorine atoms with alkynyl moieties in *N*,*N*-**III** led to the generation of highly efficient laser dyes. Also, systems with *N*,*N*- bidentate ligands other than BODIPY are known, the most relevant example being the bis(alkynyl) borane formazanate complexes *N*,*N*-**IV** reported by Gilroy [18].

Conversely, only limited reports on B(alkynyl)$_2$ compounds with *N*, *C*-bidentate ligands are known to date [19–21]. Two examples were reported by the group led by Yam [19,20] who synthesized different classes of readily tunable fluorescent dyes where the nitrogen donor atom belongs to a pyridine moiety, whereas the carbon atom bound to boron comes from a functionalized thienyl skeleton (*N*,*C*-**I** and *N*,*C*-**II**, Fig. 1). In addition, the photophysical behavior of bis(alkynyl) borane compounds were described by Harrity [21], who used ligands where both N and C donor atoms come from a pyridine fragment (*N*,*C*-**III**, Fig. 1). Worthy of note, to the best of our knowledge no B(alkynyl)$_2$

* Corresponding author.
E-mail address: stefano.brenna@uninsubria.it (S. Brenna).

https://doi.org/10.1016/j.dyepig.2023.111722
Received 5 June 2023; Received in revised form 4 September 2023; Accepted 22 September 2023
Available online 28 September 2023

compounds having *N*,*O*-bidentate ligands have been reported so far.

In our continuing research on coordination compounds with nitrogen ligands [22–25], we lately focused our attention on imidazo[1,5-*a*]pyridine scaffolds [26,27], either employed as *N*,*N*- [28–30] or *N*,*O*- [31–34] bidentate ligands. In particular, (imidazo[1,5-*a*]pyridin-3-yl) phenolates have been recently coordinated to a boron center [35–37], obtaining the corresponding boron-difluoride derivatives. These demonstrated to be a very promising class of fluorescent, blue emissive materials, displaying very large Stokes shift (0.80 eV), good photostability and high absolute quantum yields. Herein we describe the effect of replacing the fluorine atoms in our boron-difluoride compounds with aryl-acetylides, leading to bis(alkynyl) boranes which, to our knowledge, are the first ever reported bis(alkynyl) borane compounds with a *N*,*O*-bidentate ligand.

2. Results and discussion

2.1. Syntheses and characterization

The boron difluoride derivative **1** was prepared as previously described [36]. The one-pot two-steps synthesis of the bis(alkynyl) borane compounds followed a published procedure [16] (Scheme 1): first, treatment of acetylenes **2a-e** with methyl magnesium bromide afforded the corresponding acetylides, which were then reacted *in situ* with **1** to give **3a-e** as light brown solids, in moderate to good yields (see experimental part). All these bis(alkynyl)boranes are very stable in the solid state and can be stored under air for prolonged time. They also showed good stability in solution, where no degradation occurred regardless the solvent.

The infrared spectra (ATR) of all borane compounds showed a medium intensity signal at ≈2165 cm^{-1}, consistent with the presence of the C≡C triple bond (Figs. S1–S5). The ^{1}H NMR spectra of compounds **3a-e** recorded in $CDCl_3$ (Supporting Information) showed a series of resonances between 6.50 and 8.50 ppm attributed to the aromatic protons of the imidazopyridine ligand and the phenyl ring of the acetylene moiety, and a singlet around 2.40–2.70 ppm associated to the methyl group on the imidazolic ring. The corresponding resonances in the ^{13}C NMR were detected between 116 and 132 ppm (aromatic CH) and at 10–11 ppm for the methyl carbon (Supporting Information). The resonances of the alkynyl carbon atoms directly bound to boron were not detected due to coupling with the quadrupolar boron nucleus [11], whereas the other alkynyl carbon atoms were observed around 94–96 ppm. The ^{11}B NMR spectrum ($CDCl_3$, 25 °C) is characterized by a typical broad singlet centered at −6.7 ppm (Fig. S17), slightly upfield shifted compared to values reported in the literature for *N*,*N*-**I** and *N*,*C*-**II** (Fig. 1) bis(alkynyl) borane compounds.

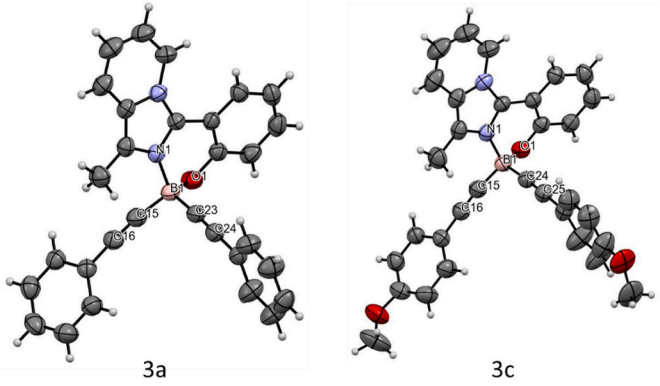

Fig. 2. ORTEP representation of **3a** and **3c** at 50% probability level, with atom labeling.

Crystals of **3a** and **3c** suitable for X-ray structure analysis were grown by slow diffusion of diethyl ether in dichloromethane. Selected bond distances and angles are reported in Table 1. In both compounds, the boron center shows the expected tetrahedral geometry, as confirmed by the calculated τ_4 indexes [38] (0.96 for **3a** and 0.95 for **3c**). The bond lengths around the boron atoms, 1.59–1.60 Å (B-N), 1.47–1.48 Å (B-O) and 1.57–1.59 Å (B-C(alkynyl)), are comparable to those reported in the literature for similar bis(alkynyl) borane compounds [11,20]. A very slight deformation on the B-C≡C connector is observed, with angles

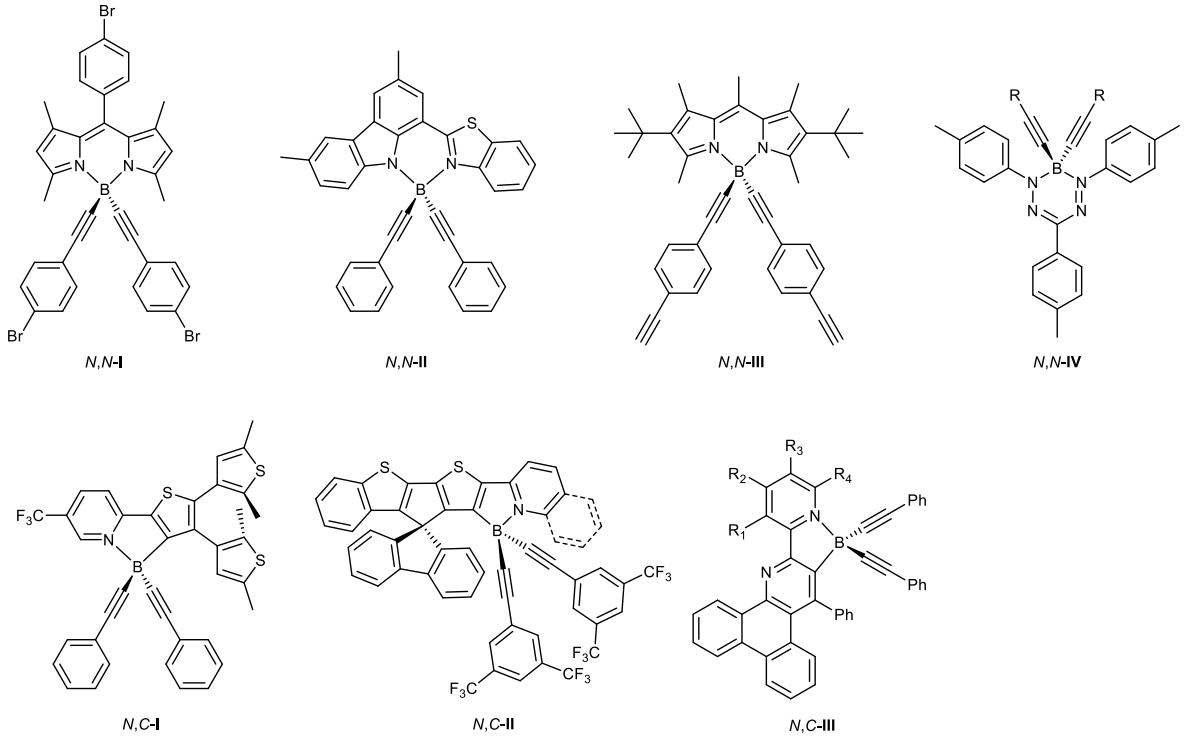

Fig. 1. Most relevant examples of bis(alkynyl) borane compounds with *N*,*N*- or *N*,*C*-bidentate ligands.

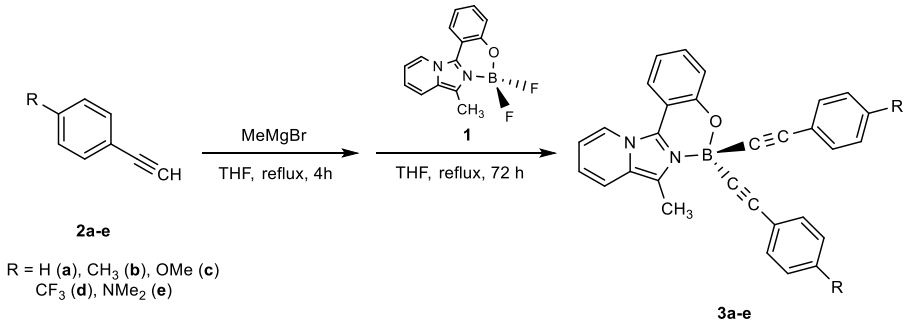

Scheme 1. One-pot two-steps synthesis of bis(alkynyl) borane compounds **3a-e**.

Table 1
Selected bond distances (Å) and angles (°) for **3a** and **3c**.

Distances (Å)		Angles (°)	
3a			
B(1)-N(1)	1.597(3)	N(1)-B(1)-O(1)	105.8(2)
B(1)-O(1)	1.468(3)	N(1)-B(1)-C(15)	112.6(2)
B(1)-C(15)	1.569(3)	N(1)-B(1)-C(23)	107.3(2)
B(1)-C(23)	1.591(3)	O(1)-B(1)-C(15)	107.7(2)
C(15)-C(16)	1.197(3)	O(1)-B(1)-C(23)	112.6(2)
C(23)-C(24)	1.206(3)	C(15)-B(1)-C(23)	110.8(2)
		B(1)-C(15)-C(16)	173.2(2)
		B(1)-C(23)-C(24)	176.2(2)
3c			
B(1)-N(1)	1.598(3)	N(1)-B(1)-O(1)	105.5(2)
B(1)-O(1)	1.476(3)	N(1)-B(1)-C(15)	113.2(2)
B(1)-C(15)	1.574(3)	N(1)-B(1)-C(24)	106.5(2)
B(1)-C(24)	1.593(3)	O(1)-B(1)-C(15)	108.7(2)
C(15)-C(16)	1.203(3)	O(1)-B(1)-C(24)	112.9(2)
C(24)-C(25)	1.206(3)	C(15)-B(1)-C(24)	110.1(2)
		B(1)-C(15)-C(16)	173.0(2)
		B(1)-C(24)-C(25)	176.5(2)

ranging from 173° to 176°. Also, the C(alkyne)-B-C(alkyne) angles, respectively measuring 110.8(2)° for **3a** and 110.1(2)° for **3c**, are comparable to those observed for structurally similar *N,N*- and *N,C*-bis (alkynyl) borane compounds [11,20]. Worthy of note, these values perfectly match those obtained by DFT calculations for the optimized ground state (S_0) of compounds **3a-3e** (*vide infra*).

3. Optical properties

All these compounds showed relevant fluorescence emission in solution, but little or no emission in the solid state; accordingly, their photophysical properties have been investigated only in solution. The absorption and emission spectra of compounds **3a-3e** are collected in Fig. 3.

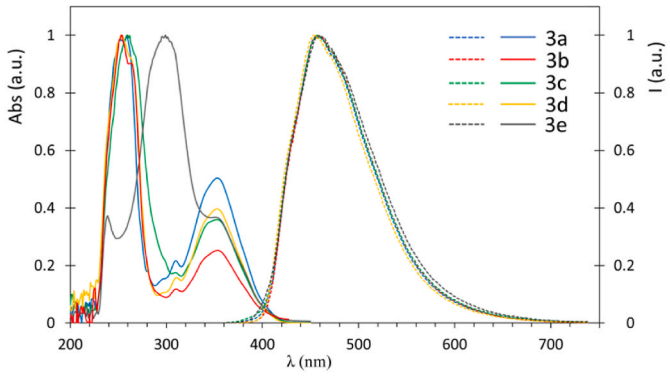

Fig. 3. Normalized absorption (full lines) and emission (dashed lines) spectra of compounds **3a-3e** recorded in solution (CH_2Cl_2, $5\bullet10^{-5}$ M).

Bis(alkynyl) borane derivatives **3a-3d** present a strong absorption at about 250 nm (π-π*) and a lower energy transition centered at about 355 nm (n- π*). In the UV–vis spectrum of compound **3e**, a bathochromic shift of the strongest absorption is observed (300 nm), whereas the second low-energy transition still appears as a shoulder at 354 nm. Thus, despite some little differences observed for **3e,** it can be concluded that there is no significant effect of substituent R of the acetylene moiety on the UV–vis spectra. The same result is noted for the emission spectra: all the derivatives show a strong, unstructured emission band in the blue region centered at about 455 nm (Fig. 3, Table 2) regardless of the substituent on the aromatic ring. Such outcomes are in accordance with what was reported for some *N,N*-bis(alkynyl) boranes [18] and for the corresponding BF_2-containing precursors [36]. However, at a deeper inspection, a slight influence of the Hammett constant σ_p of the substituent R on the emission maxima of compounds **3a-3e** was detected (Table 2). Indeed, σ_p values higher than 0 (H) lead to a slight decrease of the emission maxima, corresponding to higher values of emission expressed in cm^{-1}. The opposite effect is induced by donor substituents having σ_p values lower than 0, which produce a slight bathochromic shift of the emission. As a result, a linear correlation between the fluorescence emission (expressed in cm^{-1}) and the σ_p Hammett constant of substituent R could be derived (Fig. S18). Nevertheless, these shifts are minimal, and as already mentioned the emission maxima is always centered in the blue region (about 455 nm) for all derivatives. As expected, the presence of the (imidazo[1,5-*a*]pyridin-3-yl)phenolate ligand induces large Stokes shift (100–110 nm, ca. 0.80 eV) for all derivatives. Additionally, any possible solvent effect can be ruled out in our case: indeed, UV–vis (Fig. S19), excitation (Fig. S20) and emission spectra (Figs. S21–S25) were collected for **3a-3e** in solvents with different polarity (dichloromethane, tetrahydrofuran, chloroform, ethyl acetate, acetonitrile) and no significant differences were noticed. As an example, Fig. 4 reports the UV–vis and emission spectra collected for **3a**, whereas similar spectra for all other derivatives are reported in Figs. S19–S25 (Supporting Information). The intense blue fluorescence emission is maintained in all solvents for all derivatives, which always show a mono-exponential lifetime decay in the range 2.90–3.90 ns. Absolute fluorescence quantum yields experience a little variation according to solvent, usually being slightly lower in chloroform and acetonitrile (mainly due to lesser solubility of the bis(alkynyl) boranes in these solvents). In general, when compared to those of the corresponding BF_2-containing derivatives [36], Φ_{PL} values increase of about 20–25%, thus supporting the strategy of introducing alkynyl moieties. BODIPY-based similar compounds like those reported in Fig. 1 (*N,N*-**I** and *N,N*-**III**) and other *N,N*-containing bis(alkynyl) boranes (*N,N*-**II**) show higher quantum yields (ca. 0.40–0.45). Also thiophen-based species *N,C*-**I** and *N,C*-**II** are characterized by higher quantum yields (0.31 and 0.47 respectively). However, our compounds with imidazo[1,5-*a*] pyridin-3-yl)phenolate ligand show better performances than *N,N*-**IV** ($\Phi_{PL} < 0.5$) and *N,C*-**III** ($\Phi_{PL} = 0.12$). All the photophysical data are

Table 2
Photophysical data for compounds **3a**-**3e** recorded in dichloromethane solution and for **3a** in different solvents. All measured solutions were 5 ·10^{-5} M.

	R	σ_p	solvent	λ_{abs} (nm)	ε (M^{-1} cm^{-1})	λ_{exc} (nm)	λ_{em} (nm)	Stokes (eV)	Φ_{PL}	τ (ns)	k_r (·10^7 s^{-1})	k_{nr} (·10^8 s^{-1})
3a	H	0	CH_2Cl_2	259, 353	432394	264, 353	456	0.80	0.25	3.43	7.3	2.2
3b	Me	−0.17	CH_2Cl_2	262, 353	264077	261, 354	457	0.80	0.24	3.41	7.0	2.2
3c	OMe	−0.27	CH_2Cl_2	259, 353	312248	273, 354	457	0.79	0.23	3.29	7.0	2.3
3d	CF_3	0.54	CH_2Cl_2	253, 353	246703	263, 353	453	0.78	0.16	3.46	4.6	2.4
3e	NMe_2	−0.83	CH_2Cl_2	299, 351	415631	313, 353	459	0.81	0.17	3.36	5.1	2.5
3a	H	0	THF	264, 354	457919	266, 356	456	0.76	0.23	3.85	6.0	2.0
3a	H	0	$CHCl_3$	256, 353	409241	263, 355	459	0.79	0.06	2.91	2.1	3.2
3a	H	0	AcOEt	260, 353	458407	264, 355	454	0.76	0.12	3.65	3.3	2.4
3a	H	0	CH_3CN	257, 351	415819	262, 352	453	0.79	0.17	3.86	4.4	2.2

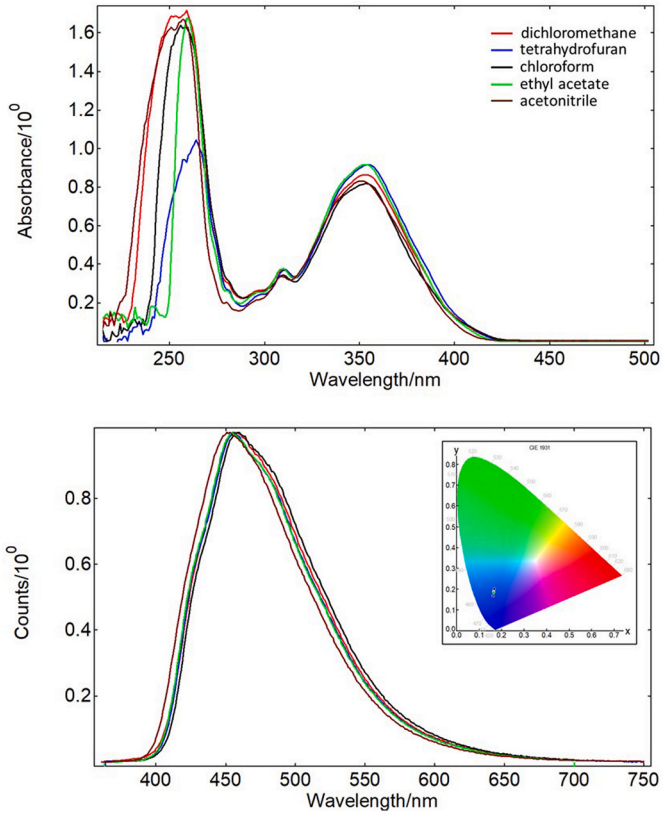

Fig. 4. Absorption (left) and emission (right) spectra of compound **3a** measured in various solvents (5•10^{-5} M). Color code: red (▬), dichloromethane; blue (▬), THF; black (▬), chloroform; green (▬), ethyl acetate; brown (▬), acetonitrile. Inset: CIE 1931 chromaticity plot for emission of compound **3a** in the different solvents.

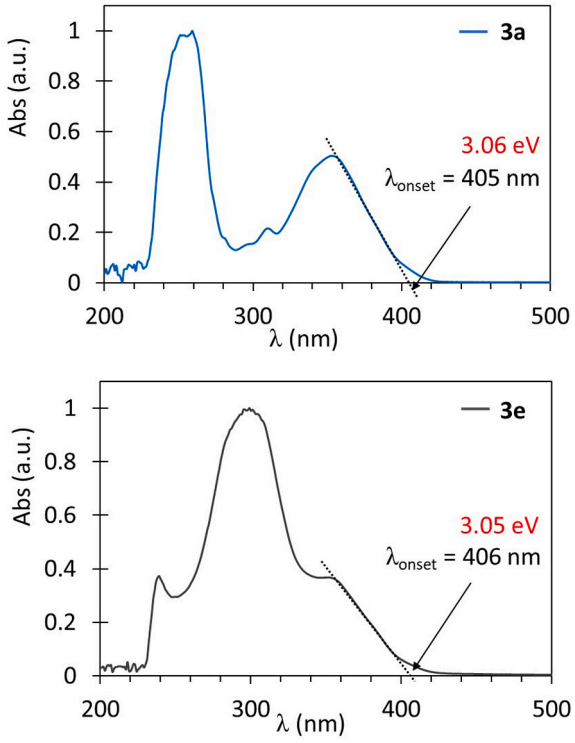

Fig. 5. UV–vis spectra of compounds **3a** and **3e** (CH_2Cl_2, 5•10^{-5} M) with the respective band gap energy estimation.

collected in Table 2 (for **3a**) and Tables S1–S5 (Supporting).

3.1. Optical band gap

The optical band gap (E_g) for molecular compounds can be approximated to the HOMO-LUMO energy difference and can be determined by extrapolation of the lower-energy absorption edge in the UV–vis spectrum, according to Eq. (1) [39]. E_g denotes the optical band gap expressed in eV whereas λ_{onset} is the absorption edge wavelength (in nm) obtained from the onset wavelength of the low energy absorption band as shown in Fig. 5.

$$E_g = h \bullet \frac{c}{\lambda_{onset}} = \frac{1240}{\lambda_{onset}\,(nm)} \qquad \text{(Eq. 1)}$$

where h is the Planck's constant and c is the speed of light in vacuum.

As an example, Fig. 5 reports the UV–vis spectra of compounds **3a** and **3e** recorded in dichloromethane, with the respective band gap energy estimation. The analogous representations for compounds **3b-3d** are reported in Fig. S26. Due to their very similar UV–vis spectra, the optical band gaps (E_g) obtained for compounds **3a-3d** as onset wavelength of the absorption at about 355 nm are nearly identical (404–406 nm, corresponding to 3.05–3.07 eV). For species **3e**, the shoulder at 354 nm in the UV–vis trace was considered, again leading to a E_g value in the same range (3.05 eV) (Fig. 5). Such identical optical band gaps can explain the comparable emission spectra recorded for **3a-3e** derivatives (Fig. 3), regardless substituent R on the acetylene moiety.

4. DFT calculations

Starting from the X-ray crystal structures of compounds **3a** and **3c**, the geometries of all the derivatives were optimized in the ground state (S_0). We first performed a benchmark experiment, using five different functionals (PBE0 [40], BLYP-D3(BJ) [41], PBE-D4(EEQ) [42], SAOP [43], M11 [44]) to acquire computed UV–vis spectra for compound **3a**. The results are summarized in Fig. S27: overall, we could conclude that there are no significant variations in the spectra calculated with the different functionals as regards the energies of the transitions, whereas major differences are noticed regarding the relative intensities of the

absorptions. We then opted for performing the following calculations using the hybrid functional PBE0, which, despite it is more time-consuming than other lighter functionals like BLYP-D3(BJ), gives a better description of the UV–vis spectra and a good agreement with experimental data [45].

Calculated and experimental (X-ray) bond distances and angles for **3a** and **3c** are in good agreement (Supporting Information for cartesian coordinates). The optimized S_0 structures present a C(alkyne)-B-C (alkyne) angle in the range 109–116° (Table S6), not so far from those measured in the crystal structure of compounds **3a** and **3c**, with slight deviations mainly due to solvent effects. TD-DFT calculations were useful to determine the nature of the transitions responsible for the absorptions: Fig. 6 reports the comparison between calculated and experimental UV–vis spectra (in dichloromethane) for compound **3a**, showing the good accordance of both intensities and position of absorption bands when calculated with the PBE0 functional. All other calculated UV–vis spectra for **3b**-**3e** are collected in Fig. S28.

The energies of the frontier molecular orbitals (HOMO-1, HOMO, LUMO, LUMO+1) for all compounds are reported in Fig. 7, whereas the major contributions of single orbital transitions to the absorption at lower energy are collected in Table S7.

Regarding the HOMO-LUMO energies (Fig. 7), the introduction of donor substituents (**3b**, **3c** and **3e**) only slightly increases the HOMO energy, whereas the LUMO is reduced (except for **3e**). This results in a little lower energy gap ($\Delta_{H\text{-}L}$) for the latter. On the contrary, the presence of the electron withdrawing CF_3 group leads to a decrease in both HOMO and LUMO energies, overall resulting in a slightly lower $\Delta_{H\text{-}L}$ when compared to **3a**.

The topologies of the frontier orbitals (HOMO-1, LUMO, LUMO+1) present some differences among the series (Fig. 8): HOMO-1 is centered on the acetylene moieties, except for **3d**, where a considerable contribution from imidazopyridine is observed. HOMO is always distributed over the nitrogen heterocycle for **3a**-**3d**, whereas for **3e** it is localized only on the $B(acet)_2$ fragment. Also considering the topologies of LUMO and LUMO+1, some differences are noticed for compound **3d** compared to the others.

Additionally, a deeper inspection of the distribution of the frontier orbitals in the molecules allowed to highlight these differences. Indeed, for **3a-3c** derivatives, the HOMO is distributed on both the imidazopyridine (60–63%) and the phenol portions (32–35%), whereas the HOMO-1 is mainly (if not entirely) localized on the $B(acet)_2$ fragment. Unoccupied orbitals are placed on the acceptor imidazopyridine scaffold (LUMO, 76–80%) and on both the imidazopyridine (>60%) and the phenol (ca. 30%) (LUMO+1). On the contrary, **3d** and **3e** compounds show a very different distribution: for the CF_3-substitued derivative **3d**, the HOMO shape is similar to the previous (**3a-3c**), but HOMO-1 has a strong prevalence of the phenol skeleton. The $B(acet)_2$ portion has major contribution in LUMO (46%) and even higher in LUMO+1 (67%). The opposite is observed for compound **3e**, bearing the strong donor substituent NMe_2: here, both HOMO and HOMO-1 are entirely localized on the $B(acet)_2$ fragment (95–98%), whereas LUMO and LUMO+1 show a predominance of the electron-withdrawing imidazopyridine moiety. All these features are well visualized in Fig. 9, whereas all the percentages are reported in Table S8 (Supporting Information).

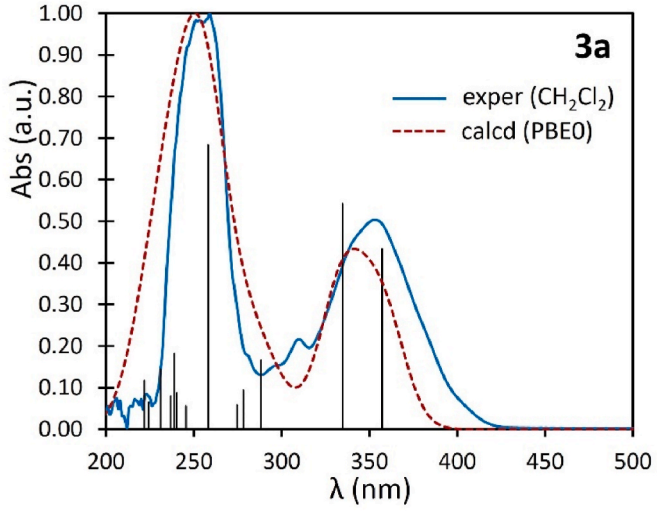

Fig. 6. Calculated *vs.* experimental UV–vis traces in dichloromethane solution for compound **3a**. Vertical bars represent calculated transitions with oscillator strength $f > 0.1$.

Next, optimization of the first singlet excited state (S_1) of compounds **3a-3e** was performed again at DFT/PBE0 level of theory: in general, a 1–2% increase in the values of the C(alkyne)-B-C(alkyne) angles is observed moving from S_0 to S_1. The Electron Density Difference Maps (EDDMs) calculated for **3a-3e** show that the electronic transition is centered on the imidazopyridine skeleton (from phenol to imidazopyridine), with no involvement of the $Bis(alkyne)_2$ fragment (Fig. 10, where electron density goes from red to green). This nearly identical shapes for EDDMs predict very similar electronic structures for all compounds, and accounts for the absence of influence of the substituent R on phenylacetylene moiety on the emission maxima of the compounds (indeed all centered at about 455 nm).

5. Experimental section

5.1. Materials and methods

Infrared Spectra (ATR) were acquired on a Thermo Scientific™ Nicolet™ iS20 FTIR Spectrometer with a 1 cm^{-1} resolution. Elemental analyses were obtained with a Perkin-Elmer CHN Analyzer 2400 Series II. NMR spectra were recorded on a Bruker AVANCEIII 400 spectrometer operating at 400 MHz for ^1H NMR, 100 MHz for $^{13}C\{^1H\}$ NMR, 376 MHz for ^{19}F and 128 MHz for ^{11}B NMR. Chemical shifts are given as δ values in ppm relative to residual solvent peaks as the internal reference. J values are given in Hz. $^{13}C\{^1H\}$ NMR spectra were acquired using an APT pulse sequence. The UV–vis, excitation and emission spectra were measured using a fluorescence spectrometer (Edinburgh Instruments FS5) equipped with a 150 W continuous Xenon lamp as a light source and were corrected for the wavelength response of the instrument; lifetime measurements were performed on the same FS5 Edinburgh Instruments using an EPLED-320 (Edinburgh Instruments) as the pulsed source. Analysis of the lifetime decay curve was done using Fluoracle® Software package (Ver. 1.9.1) which runs the FS5 instrument. Absolute fluorescence quantum yields were determined on a Photon Technology International (PTI) QuantaMaster QM-40 spectrometer (Xe arc lamp, 70 W) with a PhotoMed GmbH K-Sphere Integrating Sphere (3.2 inch. diameter). The integrated luminescence areas were obtained by the Felix32™ analysis software and used to determine the absolute PLQYs (Φ_{PL}, uncertainties of ±5%) according to the literature [46]. Acetylene **2e** was prepared according to the method reported by Karuso [47]; all other chemicals were of reagent grade quality and were purchased commercially (AlfaAesar, Acros, TCI Chemicals, Fluorochem) and used as received.

6. General procedure for the synthesis of bis(alkynyl)boranes 3a-e

In a two-necked round flask, the acetylene (15 eq.) was dissolved in 20 mL of anhydrous tetrahydrofuran. Then, 15 eq. of methylmagnesium bromide (3 M solution in diethyl ether) were slowly added dropwise. The mixture was refluxed for 4 h, then the boron difluoride compound **1** (1 eq.) was added in small portions, obtaining a deep red solution. The reaction was refluxed for 72 h, during which time the color turned to yellow, then it was cooled to room temperature and 70 mL of water were

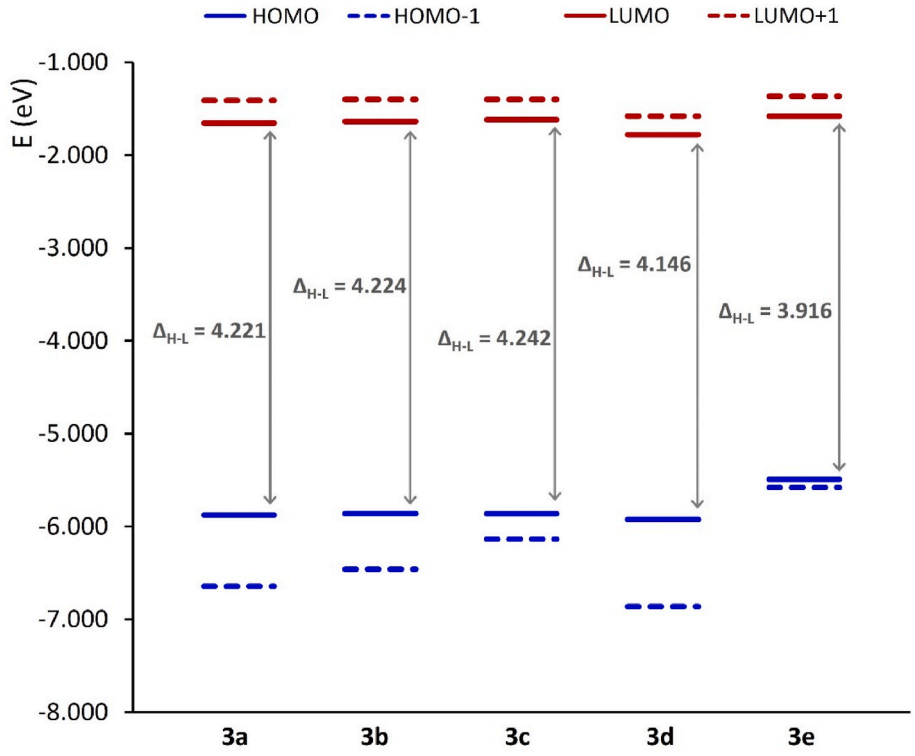

Fig. 7. Frontier molecular orbital energy levels (eV) and HOMO-LUMO energy gaps ($\Delta_{H\text{-}L}$).

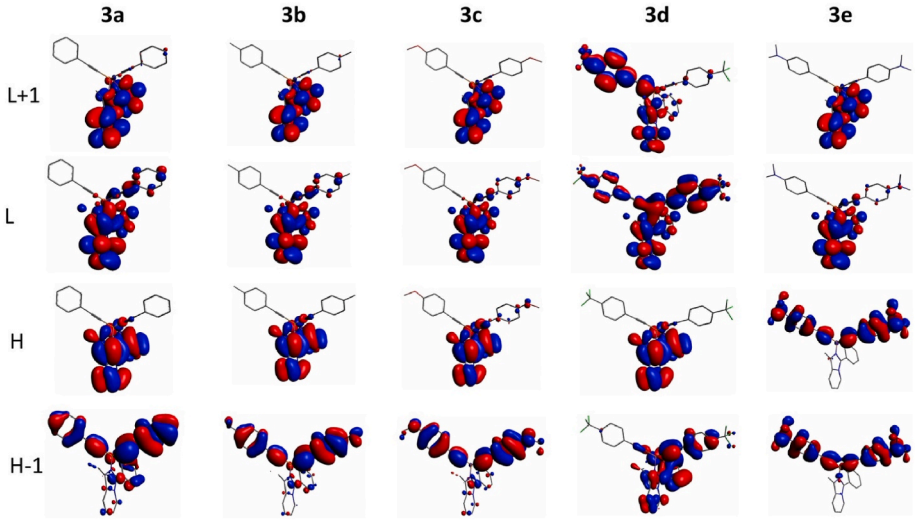

Fig. 8. Molecular orbitals shape (HOMO-1, HOMO, LUMO, LUMO+1) for compounds **3a**-**3e** calculated in dichloromethane solution.

added. The resulting mixture was extracted with dichloromethane (100 mL), dried over sodium sulphate and the solvent removed under reduced pressure to give the final product as a light brown solid.

3a: Yield: 0.36 g (75%). Anal. Calcd. (%) for $C_{30}H_{21}N_2OB$: C, 82.58; H, 4,85; N, 6,42. Found (%): C, 82.56; H, 4.98; N, 6.33. ^{1}H NMR (400 MHz, $CDCl_3$, 298 K, *J* [Hz]): δ = 8.49 (d, *J* = 6.9, 1H), 7.77 (d, *J* = 7.2, 1H), 7.55 (d, *J* = 8.6, 1H), 7.44–7.36 (m, 4H), 7.34–7.27 (m, 2H), 7.25–7.16 (m, 5H), 7.04–6.95 (m, 1H), 6.94–6.75 (m, 2H), 3.01 (s, 3H). ^{13}C NMR (101 MHz, $CDCl_3$, 298 K): δ = 156.90, 131.91, 131.79, 127.84, 127.17, 125.03, 123.84, 122.10, 121.90, 121.17, 119.93, 119.23, 119.00, 116.69, 112.31, 95.99, 10.85. ^{11}B NMR (128 MHz, $CDCl_3$, 298 K): δ = −6.70. FT-IR (ATR) (cm^{-1}): 2166 (m) C≡ C.

3b: Yield: 0.35 g (69%). Anal. Calcd. (%) for $C_{32}H_{25}N_2OB$: C, 82.77; H, 5.43; N, 6.03. Found (%): C, 82.15; H, 5.32; N, 6.13. ^{1}H NMR (400 MHz, $CDCl_3$, 298 K, *J* [Hz]): δ = 8.47 (d, *J* = 7.0, 1H), 7.75 (d, *J* = 7.2, 1H), 7.54 (d, *J* = 8.7, 1H), 7.41–7.33 (m, 2H), 7.30 (d, *J* = 8.0, 4H), 7.12 (d, *J* = 7.9, 1H), 7.04–6.98 (m, 4H), 6.96 (d, *J* = 7.1, 1H), 6.91–6.79 (m, 2H), 2.99 (s, 3H), 2.27 (d, *J* = 11.1, 6H). ^{13}C NMR (101 MHz, $CDCl_3$): δ = 157.11, 137.17, 132.17, 131.99, 131.82, 129.21, 128.75, 127.84, 122.23, 122.16, 122.04, 121.32, 119.99, 119.28, 119.14, 116.77, 96.21, 21.53, 10.99. ^{11}B NMR (128 MHz, $CDCl_3$, 298 K): δ = −6.58. FT-IR (ATR) (cm^{-1}): 2164 (m) C≡ C.

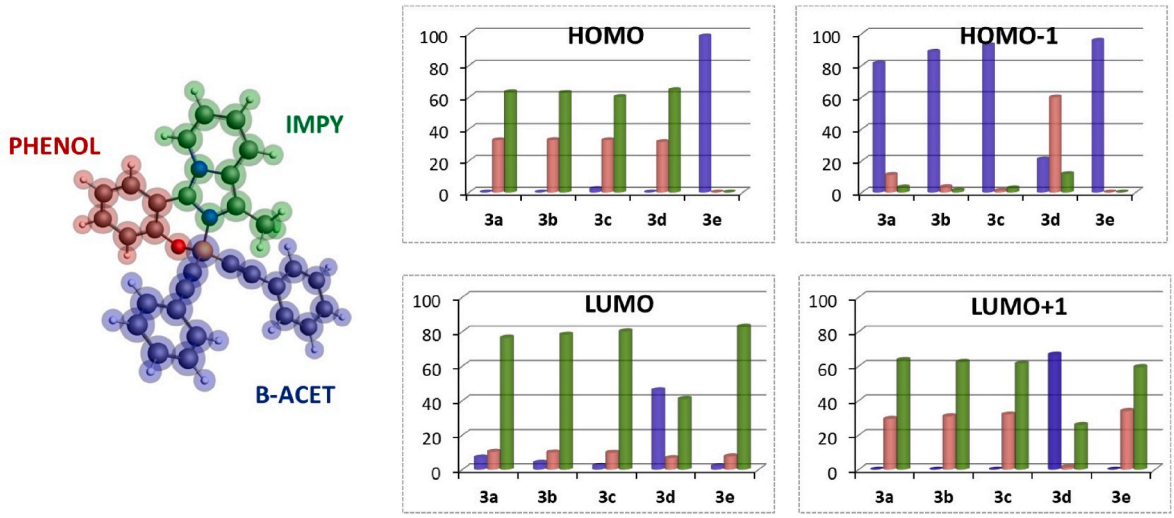

Fig. 9. Percentage contribution to frontier orbitals from the three fragments of the molecules.

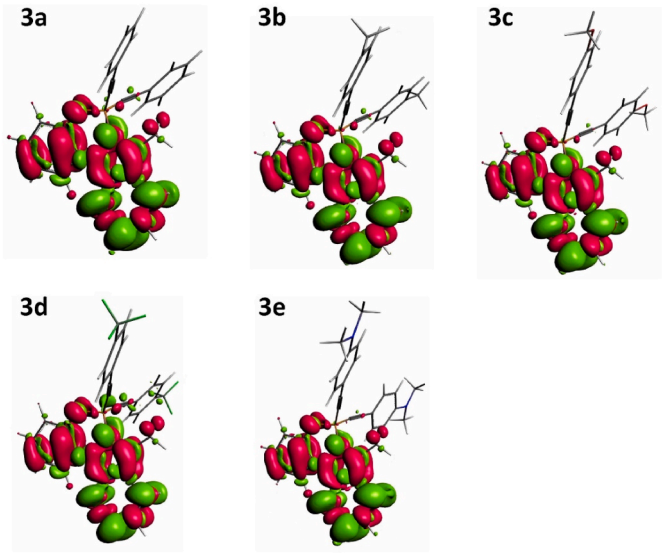

Fig. 10. Electron Difference Density Maps (EDDMs) for the lowest energy singlet electronic transition computed by TD-DFT (red indicates a decrease in electron density, green indicates an increase).

3c: Yield: 0.39 g (71%). Anal. Calcd. (%) for $C_{32}H_{25}N_2O_3B$: C, 77.43; H, 5.08; N, 5.64. Found (%): C, 77.40; H, 5.00; N, 5.81. ^{1}H NMR (400 MHz, $CDCl_3$, 298 K, *J* [Hz]): $\delta = 8.39$ (d, $J = 7.1$, 1H), 7.69 (d, $J = 7.7$, 1H), 7.49 (d, $J = 9.0$, 1H), 7.34 (d, $J = 8.7$, 4H), 7.30 (d, $J = 7.4$, 1H), 7.25 (d, $J = 7.8$, 1H), 6.91 (t, $J = 7.3$, 1H), 6.81 (m, 3H), 6.74 (d, $J = 8.7$, 4H), 3.74 (s, 6H), 2.97 (s, 3H). ^{13}C NMR (101 MHz, $CDCl_3$) δ 158.88, 156.98, 133.69, 133.21, 131.82, 127.79, 123.83, 122.15, 122.06, 121.14, 120.04, 119.16, 118.94, 116.75, 114.06, 113.61, 112.39, 95.78, 75.89, 55.29, 10.95. ^{11}B NMR (128 MHz, $CDCl_3$, 298 K): $\delta = -6.69$. FT-IR (ATR) (cm^{-1}): 2170 (m) C≡ C.

3d: Yield: 0.29 g (62%). Anal. Calcd. (%) for $C_{32}H_{19}N_2OBF_6$: C, 67.16; H, 3.35; N, 4.89. Found (%): C, 67.36; H, 3.42; N, 4.81. ^{1}H NMR (400 MHz, $CDCl_3$, 298 K, *J* [Hz]): $\delta = 8.51$ (d, $J = 7.0$, 1H), 7.79 (d, $J = 7.1$, 1H), 7.58 (d, $J = 9.7$, 1H), 7.48 (q, $J = 8.6$, 8H), 7.44–7.36 (m, 1H), 7.31 (d, $J = 7.7$, 1H), 7.07–6.98 (m, 1H), 6.95–6.86 (m, 2H), 2.99 (s, 3H). ^{13}C NMR (101 MHz, $CDCl_3$, 298 K, *J* [Hz]): $\delta = 156.68$, 132.27, 132.08, 130.83, 129.43 (q, $^2J_{CF} = 32.3$ Hz), 129.00, 128.01, 124.99 (q, $^3J_{CF} = 3.8$), 124.22 (q, $^1J_{CF} = 270.3$ Hz), 123.70, 122.27, 122.12, 121.22, 119.73, 119.14, 117.08, 112.33, 94.88, 10.96. ^{11}B NMR (128 MHz, $CDCl_3$, 298 K): $\delta = -6.87$. ^{19}F NMR (376 MHz, $CDCl_3$, 298 K): $\delta = -62.68$. FT-IR (ATR) (cm^{-1}): 2166 (m) C≡ C.

3e: Yield: 0.31 g (64%). Anal. Calcd. (%) for $C_{34}H_{31}N_4OB$: C, 78.16; H, 5.98; N, 10.72. Found (%): C, 78.22; H, 6.06; N, 10.64. ^{1}H NMR (400 MHz, $CDCl_3$, 298 K, *J* [Hz]): $\delta = 8.39$ (d, $J = 7.2$, 1H), 7.69 (d, $J = 7.8$, 1H), 7.48 (d, $J = 9.0$, 1H), 7.29 (m, $J = 8.8$, 6H), 6.90 (t, $J = 7.0$, 1H), 6.80 (m, 2H), 6.55 (d, $J = 8.8$, 4H), 2.97 (s, 3H), 2.90 (s, 12H). ^{13}C NMR (101 MHz, $CDCl_3$, 298 K, *J* [Hz]): $\delta = 157.27$, 149.56, 133.33, 132.92, 131.72, 130.73, 127.71, 124.06, 122.16, 122.02, 121.27, 119.81, 118.98, 116.59, 112.84, 112.52, 111.98, 96.70, 84.99, 11.13. ^{11}B NMR (128 MHz, $CDCl_3$, 298 K): $\delta = -6.44$. FT-IR (ATR) (cm^{-1}): 2164 (m) C≡ C.

7. Computational details

All calculations were carried out at the density functional (DFT) level of theory with the ADF2021.102 program package [48]. The PBE0 functional [40] was employed for all calculations. Frequency analyses were performed for all optimized structures to establish the nature of the stationary points. TD-DFT implemented in the ADF package was used to determine the excitation energies: the 30 lowest singlet-singlet excitations were calculated by using the optimized geometries. For geometry optimizations B, C, F, N, and O atoms were described through TZ2P basis set [triple-ξ Slater-type orbitals (STOs) plus two polarization function]. Hydrogen atoms were described through the TZP basis set [triple-ξ Slater-type orbitals (STOs) plus one polarization function]. The corresponding augmented basis sets were employed in TD-DFT calculations [49]. Restricted formalism, no-frozen-core approximation (all-electron) and no-symmetry constrains were used in all calculations. Solvent effects (CH_2Cl_2) were simulated employing the conductor-like continuum solvent model (COSMO) [50] as implemented in the ADF suite.

8. Single-crystal X-ray structure analyses

Crystals of **3a** and **3c** were mounted on a Stoe Image Plate Diffraction system equipped with a φ circle goniometer, using Mo-Kα graphite monochromated radiation ($\lambda = 0.71073$ Å) with φ range 0–200°. The structures were solved by direct methods using the program SHELXS [51], while refinement and all further calculations were carried out using SHELXL [52]. The H-atoms were included in calculated positions and treated as riding atoms using the SHELXL default parameters. The non-H atoms were refined anisotropically, using weighted full-matrix least-square on F^2. Crystallographic details are summarized in

Table S9. Fig. 2 was drawn with ORTEP–32 [53]. In **3c**, one methoxy group is disordered over two positions, with the occupancy factors being 50:50.

CCDC-2266308 (**3a**) and 2266309 (**3c**) contain the supplementary crystallographic data for this paper. These data can be obtained free of charge via www.ccdc.cam.ac.uk/data_request/cif, by e-mailing data_request@ccdc.cam.ac.uk, or by contacting The Cambridge Crystallographic Data Centre, 12, Union Road, Cambridge CB2 1EZ, UK; fax: +44 1223 336033.

9. Conclusions

In conclusion, we have described the synthesis and full characterization of five bis(alkynyl)boranes with a (imidazo[1,5-*a*]pyridine-3-yl) phenolate ligand. Both electron-donating (Me, OMe, NMe_2) and electron-withdrawing groups (CF_3) were introduced in para-position of the phenyl residue on the phenylacetylene moieties. Only a minor effect of the substituents on the photophysical properties was observed, with all compounds showing blue fluorescence emission, large Stokes shifts and good absolute quantum yields. Nevertheless, a linear correlation between the fluorescence emission and the σ_p Hammett constant of substituent R could be observed.

TD-DFT calculations performed on S_0 state were useful to define the nature of the electronic transitions involved in absorption processes (mainly a HOMO-LUMO transition), together with the contribution of single fragments to the topology of frontier orbitals. In addition, optimization of the first singlet excited state (S_1) allowed to obtain EDDMs, which gave explanation of the equal emission of the compounds in solution.

To the best of our knowledge, the present work represents the first report on bis(alkynyl)boranes containing *N*,*O*-bidentate ligands, thus paving the way to a new class of emissive boron compounds.

CRediT authorship contribution statement

Gioele Colombo: Methodology, Investigation, Data curation, Writing—Original Draft Preparation. Anita Cinco: Methodology, Investigation, Data curation, Writing—Original Draft Preparation. Stefano Brenna: Conceptualization, Methodology, Supervision, Funding Acquisition, Writing—Original Draft Preparation. Julien Furrer: Methodology, Investigation, Data curation, Writing— Review and Editing. Bruno Therrien: Methodology, Investigation, Data curation, Writing— Review and Editing. G. Attilio Ardizzoia: Conceptualization, Software, Supervision, Funding Acquisition, Writing— Review and Editing.

Declaration of competing interest

The authors declare that they have no known competing financial interests or personal relationships that could have appeared to influence the work reported in this paper.

Data availability

Data will be made available on request.

Acknowledgments

G.A.A, S.B., G.C. thank the Ministero dell'Università e della Ricerca (MUR) and the University of Insubria for funding.

This paper and related research have been partly conducted during and with the support of the Italian national inter-university PhD course in Sustainable Development and Climate change (link: www.phd-sdc.it) at the University School for Advanced Studies IUSS Pavia, Cycle XXXVIII, with the support of a scholarship financed by the Ministerial Decree no. 351 of 9th April 2022, based on the NRRP - funded by the European Union - NextGenerationEU - Mission 4 ″Education and Research", Component 1 ″Enhancement of the offer of educational services: from nurseries to universities" - Investment 4.1 "Extension of the number of research doctorates and innovative doctorates for public administration and cultural heritage" (A.C.).

Appendix A. Supplementary data

Supplementary data to this article can be found online at https://doi.org/10.1016/j.dyepig.2023.111722.

References

[1] Mallerup SL, Wang S. Boron-based stimuli responsible materials. Chem Soc Rev 2019;48:3537–49.
[2] Paramasivam K, Fialho CB, Cruz TFC, Rodrigues AI, Ferreira B, Gomes CSB, Vila-Vicosa D, Charas A, Esperança JMSS, Vieira Ferreira LF, Calhorda MJ, Maçanita AL, Morgado J, Gomes PT. New luminescent tetracoordinate boron complexes: an in-depth experimental and theoretical characterization and their application in OLEDs. Inorg Chem Front 2021;8:3930–83.
[3] Mellerup SK, Wang S. Boron-Doped molecules for optoelectronics. Trends Chem 2019;1:77–89.
[4] Vidyasagar CC, Flores BMM, Jiménez-Pérez VM, Gurubasavaraj PM. Recent advances in boron-based Schiff base derivatives for organic light-emitting diodes. Mater Today Chem 2019;11:133–55.
[5] John A, Bolte M, Lerner HW, Meng G, Wang S, Peng T, Wagner M. Doubly boron-doped pentacenes as emitters for OLEDs. J Mater Chem C 2018;6:10881–7.
[6] Ji L, Griesbeck S, Marder TB. Recent developments in and perspectives on three-coordinate boron materials: a bright future. Chem Sci 2017;8:846–63.
[7] Berger SM, Marder TB. Applications of triarylborane materials in cell imaging and sensing of bio-relevant molecules such as DNA, RNA, and proteins. Mater Horiz 2022;9:112–20.
[8] Lara-Cerón JA, Jiménez Pérez VM, Xochicale-Santana L, Ochoa ME, Chávez-Reyes A, Muñoz-Flores BM. Boron Schiff bases derived from α-amino acids as nucleoli/cytoplasm cell-staining fluorescent probes in vitro. RSC Adv 2020;10:31748–57.
[9] Loudet A, Burgess K. BODIPY dyes and their derivatives: syntheses and spectroscopic properties. Chem Rev 2007;107:4891–932.
[10] Ulrich G, Goze C, Guardigli M, Roda A, Ziessel R. Pyrromethene dialkynyl borane complexes for "cascatelle" energy transfer and protein labeling. Angew Chem Int Ed 2005;44:3694–8.
[11] Goze C, Ulrich G, Ziessel R. Tetrahedral boron chemistry for the preparation of highly efficient "cascatelle" devices. J Org Chem 2007;72:313–22.
[12] Kaloudi-Chantzea A, Karakostas N, Pitterl F, Raptopoulou CP, Glezos N, Pistolis G. Efficient supramolecular synthesis of a robust circular light-harvesting Bodipy-dye based array. Chem Commun 2012;48:12213–5.
[13] Jiang XD, Fu Y, Zhang T, Zhao W. Synthesis and properties of NIR aza-BODIPYs with aryl and alkynyl substituents on the boron center. Tetrahedron Lett 2012;53:5703–6.
[14] Ziessel R, Ulrich G, Haefele A, Harriman A. An artificial light-harvesting array constructed from multiple bodipy dyes. J Am Chem Soc 2013;135:11330–44.
[15] Duran-Sampedro G, Esnal I, Agarrabeitia AR, Bañuelos Prieto J, Cerdán L, García-Moreno I, Costela A, Lopez-Arbeloa I, Ortiz MJ. First highly efficient and photostable E and C derivatives of 4,4-difluoro-4-bora-3a,4a-diaza-s-indacene (BODIPY) as dye lasers in the liquid phase, thin films and solid-state rods. Chem Eur J 2014;20:2646–53.
[16] Maeda C, Nagahata K, Ema T. Carbazole-based BODIPYs with ethynyl substituents at the boron center: solid-state excimer fluorescence in the VIS/NIR region. Org Biomol Chem 2017;15:7783–8.
[17] Atilgan A, Cetin MM, Yu J, Beldjoudi Y, Stern CL, Cetin FM, Islamoglu T, Farha OK, Deria P, Stoddart JF, Hupp JT. Post-synthetically elaborated BODIPY-based porous organic polymers (POPs) for the photochemical detoxification of a sulfur mustard simulant. J Am Chem Soc 2020;142:18554–64.
[18] Van Belois A, Maar RR, Workentin MS, Gilroy JB. Dialkynylborane complexes of formazanate ligands: synthesis, electronic properties, and reactivity. Inorg Chem 2019;58:834–43.
[19] Wong HL, Wong WT, Yam VWW. Photochromic thienylpyridine-bis (alkynyl) borane complexes: toward readily tunable fluorescence dyes and photoswitchable materials. Org Lett 2012;14:1862–5.
[20] Wong BYW, Wong HL, Wong YC, Chan MY, Yam VWW. Air-stable spirofluorene-containing ladder-type bis(alkynyl) borane compounds with readily tunable full color emission properties. Chem Eur J 2016;22:15095–106.
[21] Bachollet SPJT, Volz D, Fiser B, Münch S, Rönicke F, Carrillo J, Adams H, Schepers U, Gómez-Bengoa E, Bräse S, Harrity JPA. A modular class of fluorescent difluoroboranes: synthesis, structure, optical properties, theoretical calculations and applications for biological imaging. Chem Eur J 2016;22:12430–8.
[22] Ardizzoia GA, Brenna S, Therrien B. The adaptable coordination chemistry of 6-chloro-2-(quinolin-2-yl)-2,4-dihydro-1H-benzo[d][1,3]oxazine towards zinc(II) and mercury(II). Eur J Inorg Chem 2010;21:3365–71.
[23] Ardizzoia GA, Brenna S, Durini S, Trentin I, Therrien B. The Goldilocks principle in action: synthesis and structural characterization of a novel $\{Cu_4(\mu_3\text{-}OH)_4\}$ cubane stabilized by monodentate ligands. Dalton Trans 2013;42:12265–73.
[24] Ardizzoia GA, Bea M, Brenna S, Therrien B. A quantitative description of the σ-donor and π-acceptor properties of substituted phenanthrolines. Eur J Inorg Chem 2016;23:3829–37.

[25] Ardizzoia GA, Brenna S, Civati F, Colombo V, Sironi A. A phosphorescent copper (I) coordination polymer with sodium 3,5-dimethyl-4-sulfonate pyrazolate. CrystEngComm 2017;19:6020–7.

[26] Marchesi A, Brenna S, Ardizzoia GA. Synthesis and emissive properties of a series of tetrahydro (imidazo[1,5-a]pyrid-3-yl)phenols: a new class of large Stokes shift organic dyes. Dyes Pigments 2019;161:457–63.

[27] Colombo G, Ardizzoia GA, Brenna S. Imidazo[1,5-a]pyridine-based derivatives as highly fluorescent dyes. Inorg Chim Acta 2022;535:120849–63.

[28] Ardizzoia GA, Brenna S, Durini S, Therrien B, Veronelli M. Synthesis, structure, and photophysical properties of blue-emitting zinc(II) complexes with 3-aryl-substituted 1-pyridylimidazo[1,5-a]pyridine ligands. Eur J Inorg Chem 2014;26:4310–9.

[29] Ardizzoia GA, Brenna S, Durini S, Therrien B. Synthesis and characterization of luminescent zinc (II) complexes of a N,N-bidentate 1-pyridylimidazo[1,5-a]pyridine ligand. Polyhedron 2015;90:214–20.

[30] Durini S, Ardizzoia GA, Therrien B, Brenna S. Tuning the fluorescence emission in mononuclear heteroleptic trigonal silver (I) complexes. New J Chem 2017;41:3006–14.

[31] Ardizzoia GA, Ghiotti D, Therrien B, Brenna S. Homoleptic complexes of divalent metals bearing N,O-bidentate imidazo[1,5-a]pyridine ligands: synthesis, x-ray characterization and catalytic activity in the Heck reaction. Inorg Chim Acta 2018;471:384–90.

[32] Ardizzoia GA, Colombo G, Therrien B, Brenna S. Tuning the fluorescence emission and HOMO-LUMO band gap in homoleptic zinc(II) complexes with N,O-bidentate (imidazo[1,5-a]pyrid-3-yl)phenols. Eur J Inorg Chem 2019;13:1825–31.

[33] Strianese M, Brenna S, Ardizzoia GA, Guarnieri D, Lamberti M, D'Auria I, Pellecchia C. Imidazo-pyridine-based zinc (II) complexes as fluorescent hydrogen sulfide probes. Dalton Trans 2021;50:17075–85.

[34] D'Alterio MC, D'Auria I, Tedesco C, Brenna S, Pellecchia C. Are well performing catalysts for the ring opening polymerization of L-lactide under mild laboratory conditions suitable for the industrial process? The case of new highly active zinc(II) catalysts. Macromolecules 2022;55:5115–22.

[35] Colombo G, Romeo A, Ardizzoia GA, Furrer J, Therrien B, Brenna S. Boron difluoride functionalized (tetrahydroimidazo[1,5-a]pyridine-3-yl) phenols: highly fluorescent blue emissive materials. Dyes Pigments 2020;182:108636–44.

[36] Colombo G, Ardizzoia GA, Furrer J, Therrien B, Brenna S. Driving the emission towards blue by controlling the HOMO-LUMO energy gap in BF_2-functionalized 2-(imidazo[1,5-a]pyridin-3-yl)phenols. Chem Eur J 2021;27:12380–7.

[37] Colombo G, Cinco A, Ardizzoia GA, Brenna S. Long-alkyl chain functionalized imidazo[1,5-a]pyridine derivatives as blue emissive dyes. Colorants 2023;2:179–93.

[38] Yang L, Powell DR, Houser RP. Structural variation in copper (I) complexes with pyridylmethylamide ligands: structural analysis with a new four-coordinate geometry index τ_4. Dalton Trans 2007:955–64.

[39] a) López-Mayorga B, Sandoval-Chávez CI, Carreón-Castro P, Ugalde-Saldívar VM, Cortés-Guzmán F, López-Cortés JG, Ortega-Alfaro MC. Ferrocene amphiphilic D-π-A dyes: synthesis, redox behavior and determination of band gaps. New J Chem 2018;42:6101–13.b) Costa JCS, Taveira RJS, Lima CFRAC, Mendes A, Santos LMNBF. Optical band gaps of organic semiconductor materials. Opt Mater 2016;58:51–60.

[40] Adamo C, Scuseria GE, Barone V. Accurate excitation energies from time-dependent density functional theory: assessing the PBE0 model. J Chem Phys 1999;111:2889–99.

[41] Grimme S, Antony J, Ehrlich S, Krieg H. A consistent and accurate ab initio parametrization of density functional dispersion correction (DFT-D) for the 94 elements H-Pu. J Chem Phys 2010;132:154104.

[42] Caldeweyher E, Ehlert S, Hansen A, Neugebauer H, Spicher S, Banwarth C, Grimme S. A generally applicable atomic-charge dependent London dispersion correction. J Chem Phys 2019;150:154122.

[43] Shipper PRT, Gritsenko OV, van Gisbergen SJA, Baerends EJ. Molecular calculations of excitation energies and (hyper)polarizabilities with a statistical average of orbital model exchange-correlation potentials. J Chem Phys 2000;112:1344–52.

[44] Peverati R, Truhlar DG. Improving the accuracy of hybrid meta-GGA density functionals by range separation. J Phys Chem Lett 2011;2:2810–7.

[45] Worthy of note, in the initial stage of the study we performed DFT calculations on first singlet excited state (S_1) of compounds **3a-3e** using BLYP-D3(BJ) functional, which however led to some discrepancies between experimental data and theoretical calculations. In particular, geometries optimized with BLYP-D3(BJ) resulted in some critical distortions in the excited state for derivatives **3c, 3d** and **3e**, thus not allowing for a precise description of the emissive properties of our compounds. For the sake of completeness, we added the EDDMs calculated by BLYP-D3(BJ) in Supporting (Figure S29). Then, constructive criticism by one Reviewer about these discrepancies, spurred us to investigate the problem by performing further calculations, ultimately leading to the nice results obtained with the PBE0 functional.

[46] Pålsson LO, Monkman AP. Measurements of solid-state photoluminescence quantum yields of films using a fluorimeter. Adv Mater 2002;14:757–8.

[47] Cleeman F, Kum-Cheung WL, Karuso P. Combinatorial synthesis of new fluorescent scaffolds using click chemistry. Tetrahedron Lett 2022;88:153520–4.

[48] a) Te Velde G, Bickelhaupt FM, Baerends EJ, Fonseca Guerra C, van Gisbergen SJA, Snijders JG, Ziegler T. Chemistry with ADF. J Comput Chem 2021;22:931–67.b) Fonseca Guerra C, Snijders JG, te Velde G, Baerends EJ. Towards an order-N DFT method. Theor Chem Acc 1998;99:391–403.c) Baerends EJ, Ziegler T, Autschbach J, Bashford D, Bérces A, Bickelhaupt FM, Bo C, Boerrigter PM, Cavallo L, Chong DP, Deng L, Dickson RM, Ellis DE, van Faassen M, Fan L, Fischer TH, Fonseca Guerra C, Franchini M, Ghysels A, Giammona A, van Gisbergen SJA, Götz AW, Groeneveld JA, Gritsenko OV, Grüning M, Gusarov S, Harris FE, van den Hoek P, Jacob CR, Jacobsen H, Jensen L, Kaminski JW, van Kessel G, Kootstra F, Kovalenko A, Krykunov MV, van Lenthe E, McCormack DA, Michalak A, Mitoraj M, Morton SM, Neugebauer J, Nicu VP, Noodleman L, Osinga VP, Patchkovskii S, Pavanello M, Philipsen PHT, Post D, Pye CC, Ravenek W, Rodríguez JI, Ros P, Schipper PRT, van Schoot H, Schreckenbach G, Seldenthuis JS, Seth M, Snijders JG, Solà M, Swart M, Swerhone D, te Velde G, Vernooijs P, Versluis L, Visscher L, Visser O, Wang F, Wesolowski TA, van Wezenbeek EM, Wiesenekker G, Wolff SK, Woo TK, Yakovlev AL. SCM, theoretical chemistry. ADF. Amsterdam, The Netherlands: Vrije Universiteit; 2014. http://www.scm.com.

[49] Chong DP. Augmenting basis set for time-dependent density functional theory calculation of excitation energies. Slater-type orbitals for hydrogen to krypton 2005;103:749–61.

[50] a) Klamt A, Schürmann GJ. COSMO: a new approach to dielectric screening in solvents with explicit expressions for the screening energy and its gradient. J. Chem. Soc. Perkin Trans. 1993;2:799–805.b) Klamt A, Jonas V. Treatment of the outlying charge in continuum solvation models. J Chem Phys 1996;105:9972–81.c) Pye CC, Ziegler T. An implementation of the conductor-like screening model of solvation withing the Amsterdam density functional package. Theor Chem Acc 1999;101:396–408.

[51] Sheldrick GM. Phase annealing in SHELX-90: direct methods for larger structures. Acta Crystallogr 1990;A46:467–73.

[52] Sheldrick GM. Crystal structure refinement with SHELXL. Acta Crystallogr 2015;C71:3–8.

[53] Farrugia LJ. ORTEP-3 for windows - a version of ORTEP-III with a graphical user interface (GUI). J Appl Crystallogr 1997;30:565.